JOURNAL OF PROPULSION AND POWER
Vol. 26, No. 5, September–October 2010

Model for Melt-Layer Front in Ammonium Perchlorate Propellant Combustion

Taeyong Jung* and Jack J. Yoh†
Seoul National University, Seoul 151-744, Republic of Korea

DOI: 10.2514/1.47884

In solid rocket-propellant combustion, the dynamic phase change from condensed to gas occurs across the melt layer. During the surface burning, liquid and gas phases are mixed in the intermediate zone between the propellant and the flame to form microscale bubbles. The known thickness of the entire melt layer is approximately 1 μm at 10^5 Pa and 0.1 μm at approximately 10^7 Pa for ammonium-perchlorate/hydroxy-terminated polybutadiene propellant. In this paper, a model of the melt-layer front between the condensed and gaseous phases and the dynamic motion of the melt-layer front derived from the classical phase-field theory is presented. The model results show that the melt-layer front grows and propagates uniformly according to $\exp(-1/T_s)$, with T_s being the propellant surface temperature.

Nomenclature

A	=	preexponential factor, cm/s
B_φ	=	multiplication factor
c_p	=	specific pressure heat capacity, kJ/kg · K
c_v	=	specific volume heat capacity, kJ/kg · K
E_a	=	activation energy, kcal/mol
k	=	thermal conductivity, W/m · K
p	=	pressure, Pa
Q_C	=	heat of combustion, kJ/kg
Q_m	=	heat of melting, kJ/kg
Q_v	=	heat of vaporization, kJ/kg
R	=	gas constant
R_g	=	gas constant at gas phase
R_l	=	gas constant at liquid phase
r_i	=	burning rate of ith reaction
T	=	temperature, K
T_s	=	surface temperature, K
T_v	=	vaporization temperature, K
u	=	velocity, m/s
Y	=	mass fraction
β_c	=	enthalpy transition function
γ_φ	=	phase diffusion coefficient, kg m/s^2
λ_g	=	heat conductivity of gas phase, W/m · K
μ_f	=	viscosity coefficient, kg/m · s
ρ	=	density, kg/m^3
φ	=	phase variable
ψ	=	phase well depth

I. Introduction

AMMONIUM perchlorate (AP) has been used as a common oxidizer of rocket propellant because of its known stability with respect to combustion and its burning rate that can be controlled by varying the AP particle-size distribution, which is a major difference from nitramines such as cyclotrimethylenetrinitramine (RDX) or octahydrotetranitrotetrazine HMX. Hydroxyl-terminated polybutadiene (HTPB) has been a common polymeric binder/fuel in the AP-based solid rocket propellants.

The propellant surface is usually assumed to be nonuniform, because the surface is a mixture of oxidizer and binder grains for which the microscopic structures and sizes vary. Hermance [1] considered this structural feature of propellant and proposed a statistical combustion model where the propellant surface condition was considered. Beckstead et al. [2] modified and complemented [1] by suggesting a model of a multiflame structure that included premixed flame, primary flame, and final diffusion flame, called the BDP (Beckstead–Derr–Price) model, as shown in Fig. 1. Both models considered the condensed-phase decomposition of the propellant before generation of product gases. The BDP model builds a mixed (condensed and gaseous) structure from various sets of chemical-reaction mechanisms.

There have been a series of variant BDP models of AP/HTPB composite propellant known to this date. Hegab et al. [3] showed two-step kinetics that are made up of a premixed flame and a final diffusion flame. Massa et al. [4] showed a three-step kinetic model that included all BDP flames. The premixed flame is formed by the decomposition process of AP, the primary diffusion flame consists of a mixture of AP and HTPB, and the final diffusion flame consists of the product gases produced from decomposition of AP and HTPB.

The chemical process of an AP/HTPB composite propellant includes melting and surface pyrolysis, condensed-phase heating, degradation of AP/HTPB, and gas phase reactions [5]. In the performance evaluation of a rocket propellant, thrust is an important measure based on mass flux. Since mass flux is determined by the propellant's burning rate, careful estimation of the burning rate has been the central interest in the study of propellant combustion.

References [6,7] suggest that the thermal decomposition process of AP is a dissociative sublimation, described by Eq. (1):

$$\mathrm{AP}\,(s) \rightarrow \mathrm{NH_3}(g) + \mathrm{HClO_4}(g) \tag{1}$$

where there is no liquid state of combustion during the proposed process. Reference [8], on the other hand, included the condensed-phase reaction and extended this equation into the following form:

$$\mathrm{AP}\,(s) \rightarrow \mathrm{AP}(l) \rightarrow \mathrm{NH_3}(g) + \mathrm{HClO_4}(g) \tag{2}$$

Here, the liquid phase of AP, noted AP (l), is included during the gas production process of Eq. (2). The phase change occurs readily in the melt region between condensed and gas, where microstructured bubbles form on the propellant surface. Figure 2 shows a concept of melt-layer growth during solid propellant burning. The affect of this layer on propellant combustion is not fully known; thus, the specifics on its structure and dynamics require a closer look.

Received 29 October 2009; revision received 31 May 2010; accepted for publication 7 June 2010.

*School of Mechanical and Aerospace Engineering, 599 Gwanak-Ro, Gwanak-Gu.

†Associate Professor, School of Mechanical and Aerospace Engineering, 599 Gwanak-Ro, Gwanak-Gu; jjyoh@snu.ac.kr. Member AIAA.

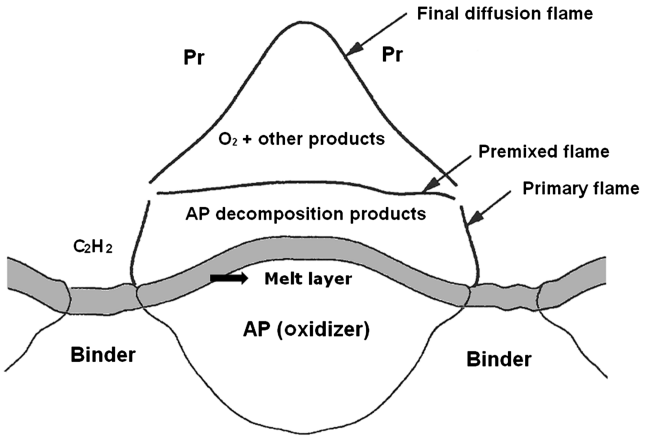

Fig. 1 Modified BDP model showing AP decomposition product layer (in dark band) where the condensed state of combustion occurs.

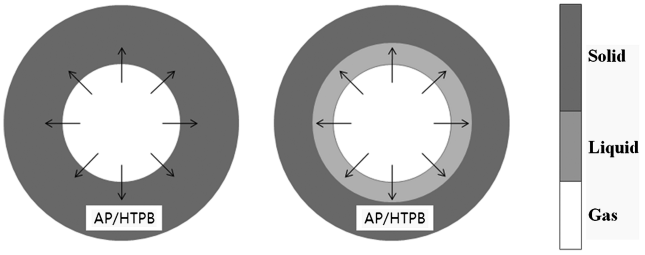

Fig. 2 Concept of melt-layer growth in solid rocket propellant. The melt-layer front is the interface between liquid and gas.

In this paper, we propose a method for estimating 1) the melt-layer-front thickness and 2) the burning rate of AP/HTPB propellant by the phase-field approach. The melt-layer front is an interface between the condensed and gaseous phases of burning propellant. The melt-layer front of AP/HTPB may have a different thickness when compared with that of AP monopropellant, but the presence of AP particles in both cases affects the thickness more so than the binder content alone. Since the melt-layer front is on the order of 10^{-2} μ during the combustion at a high-pressure condition, we will make no distinction between the AP monopropellant and the AP/HTPB propellant in the front-layer thickness estimation.

Amongst the several phase models and theories known over the years, the Ginzburg–Landau and Cahn–Hilliard models have been well received for their simplicity and physical soundness. However, they limit the manner in which rate terms are entered into equations, requiring a priori specification of the constitutive equations. The phase-change model based on a configurational force balance proposed by Gurtin [9] is adopted in the present approach. The model consists of both the microforce balance at the phase interface and the second law (Clausius–Duhem inequality) of thermodynamics. The proposed model captures the process of initiation, growth, and propagation of the melt-layer front. The propagation speed is equal to an empirical rate proportional to$\exp(-1/T_s)$.

II. Melt-Layer-Front Modeling by Phase Equation

A. Motivation for Condensed and Gaseous Phase Modeling

Summerfield et al. [10] reported that the burning surface of AP propellants is dry; there is no intermediate layer between the flame and the propellant, contrary to HMX and RDX [11,12]. (Reference [13] shows the calculated phase front thickness of HMX via the phase-field approach.) If there exists a melt layer, fuel and oxidant gases would be present, and they would enter the gaseous reaction zone under the premixed condition. Figure 3 shows a photographic image of the reaction zone and a thin layer that separates the gaseous region from the condensed side. The existence of a melt layer is proposed by several researchers [8,14,15]; they made reference to the melt layer and estimated its thickness. Accordingly, the burning is accompanied by the growth of the melt-layer front between the condensed and the gaseous regions of the propellant. We develop a modeling strategy and outline the governing equations of multiphase propellant combustion.

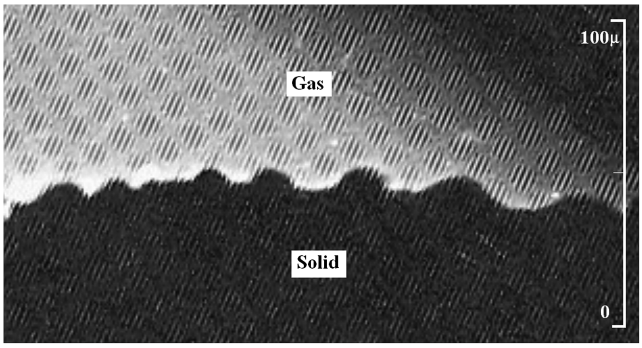

Fig. 3 Burn surface image of AP propellant from experiment [10] showing the regression layer between solid and gas.

B. Governing Equations

The one-dimensional equations for propellant with two distinct phases (condensed and gaseous) are described [13,16]. Since the equation of motion has to account for the gaseous states, the deformation of propellant is ignored. The mass, momentum, energy, and phase-field equations are

$$\frac{\partial \rho}{\partial t} + u\frac{\partial \rho}{\partial x} + \rho\frac{\partial u}{\partial x} = 0 \tag{3}$$

$$\rho\left(\frac{\partial u}{\partial t} + u\frac{\partial u}{\partial x}\right) = \frac{\partial}{\partial x}\left[-\rho RT - \rho\gamma_\varphi\left(\frac{\partial \varphi}{\partial x}\right)^2 + \frac{4}{3}\mu_f\frac{\partial u}{\partial x}\right] \tag{4}$$

$$\rho c_v\left(\frac{\partial T}{\partial t} + u\frac{\partial T}{\partial x}\right) = k\frac{\partial^2 T}{\partial x^2} + \frac{4}{3}\mu_f\left(\frac{\partial u}{\partial x}\right)^2 - p\frac{\partial u}{\partial x} + T\rho\left(\beta_v'\frac{Q_v}{T_v}\right)\dot{\varphi} + B_\varphi\dot{\varphi}^2 + \sum_1^N Q_n r_n \tag{5}$$

$$B_\varphi\left(\frac{\mathrm{d}\varphi}{\mathrm{d}t} + u\frac{\mathrm{d}\varphi}{\mathrm{d}x}\right) = \rho\gamma_\varphi\frac{\partial^2\varphi}{\partial x^2} - \rho\frac{1}{2}\Psi\frac{\partial}{\partial\varphi}\{[(\varphi-1)(\varphi-2)]^2\} - \rho\beta_v'(\varphi)\frac{T-T_v}{T_v}Q_v \tag{6}$$

Equations (3–5) are the conservation equations of mass, momentum, and energy. The phase-field evolution in Eq. (6) governs the phase state of the propellant during the dynamic surface burning. $\Psi > 0$ is a constant that describes the depth of the phase potential function, and $Q_v < 0$ is the endothermic enthalpy of vaporization. The range of the phase variable is bounded between 1 and 2, where $\varphi = 1$ a condensed state and $\varphi = 2$ a gas state. The double well potential $[(\varphi-1)(\varphi-2)]^2$ has two stable roots at each phase at $\varphi = 1$, a condensed phase, and at $\varphi = 2$, a gas phase. Any metastable phase between two stable roots naturally tends to a stable root. The transition function that ensures smooth variable transition between the stable roots is $\beta_v'(\varphi)$, as defined in the Appendix. The gas constant R of the equation of state is designed to assume a single phase and transform to another phase state of the propellant. All other phase transfer functions are summarized in the Appendix.

C. Steady-State Calculation of Melt-Layer-Front Structure

The standard procedure for obtaining a set of steady equations from the general unsteady equations requires use of a transformation

coordinate system that moves with the phase velocity D. The transformation coordinate ξ and the transformed velocity U, with respect to the particle velocity u, are defined as $\xi = x - Dt$ and $U = u - D$. Analytical description of a steady-wave system requires writing the conservation equations as a set of first-order ordinary differential equations as follows:

$$\frac{\mathrm{d}U}{\mathrm{d}\xi} = \frac{3}{4\mu_f}(mU + p + \rho\gamma_\varphi G^2 - p_\infty) \tag{7}$$

$$\frac{\mathrm{d}T}{\mathrm{d}\xi} = H \tag{8}$$

$$\frac{\mathrm{d}H}{\mathrm{d}\xi} = \frac{1}{k}\left[mc_v\frac{\partial T}{\partial \xi} - \frac{4}{3}\mu_f\left(\frac{\mathrm{d}U}{\mathrm{d}\xi}\right)^2 + \rho RT\frac{\mathrm{d}U}{\mathrm{d}\xi} - \rho T\beta_v'(\varphi)\frac{Q_v}{T_v}UG + Q_c\beta_c\right] \tag{9}$$

$$\frac{\mathrm{d}\varphi}{\mathrm{d}\xi} = G \tag{10}$$

$$\frac{\mathrm{d}G}{\mathrm{d}\xi} = \frac{1}{\gamma_\varphi}\left[\frac{GB_\varphi U}{\rho} + \frac{1}{2}\Psi\frac{\partial}{\partial\varphi}\{[\varphi(\varphi-1)(\varphi-2)]^2\} + \beta_v'(\varphi)\frac{T-T_v}{T_v}Q_v\right] \tag{11}$$

with $m = \rho u$ from the mass conservation. The variables H and G, from Eqs. (8) and (10), are used to formulate the first-order system of ordinary differential equations, as in the classical Rankine–Hugoniot shock structure analysis. Reference [13] provides the extent to which the present formulation has been applied in understanding the phase structure of HMX.

Instead of solving a full chemical kinetics, a total energy added to the system due to chemical reaction, $Q_c\beta_c$, effectively replaces the rate of enthalpy rise due to individual chemical reactions summed over N number of reactions:

$$\sum_{i=1}^{N} Q_i r_i$$

as shown in Eq. (5). When $Q_c\beta_c$ is calculated, β_c effectively sets the mass fraction of AP to be 0.88 and HTPB to be 0.12. The value of

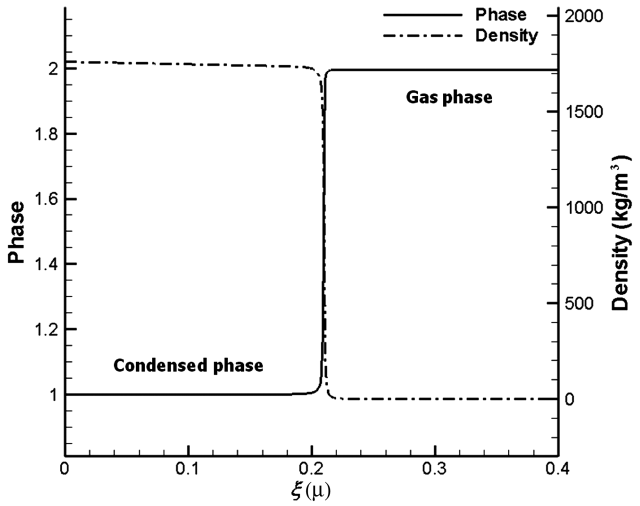

Fig. 4 Calculated steady-state melt-layer-front structure of AP/HTPB propellant. Estimated front thickness is on the order of 10^{-2} μ, approximately one-tenth of a measured whole layer thickness.

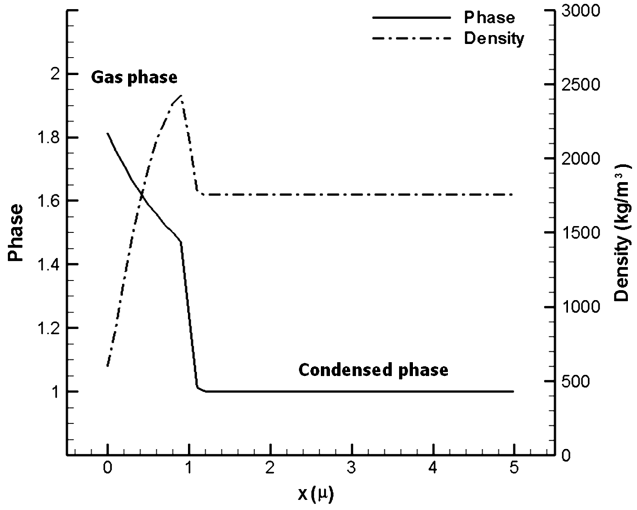

Fig. 5 Initiation of melt-layer front.

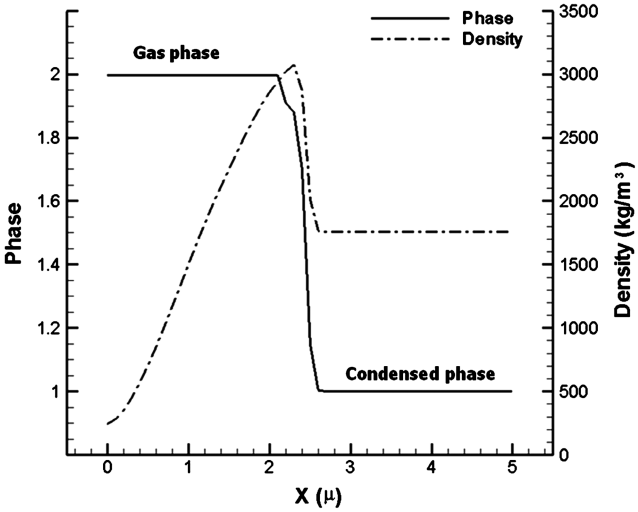

Fig. 6 Growth of propagating melt-layer front.

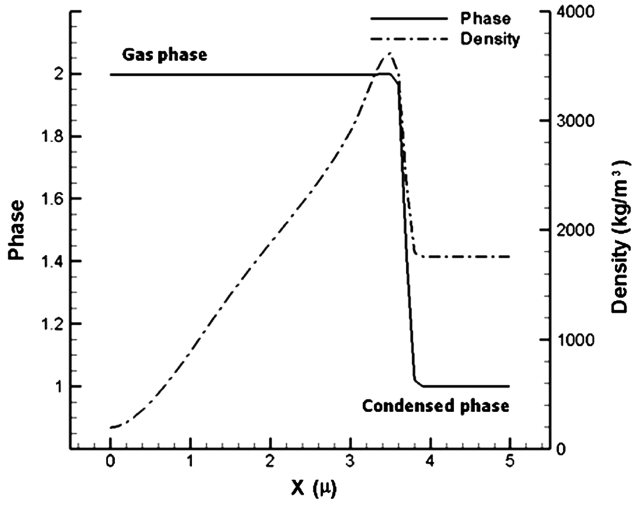

Fig. 7 Propagation of melt-layer front.

Table 1 Parameters for steady melt-layer-front structure calculation

Parameter	Value	Parameter	Value
ρ_1	1800 kg/m^3	m	1.8 kg/m^2-s
u_1	0.001 m/s	Q_v	−1800 kJ/kg
T_1	860 K	c_v	1 kJ/kg · K
φ_1	10^{-4}	κ	0.4 W/m · K
T_v	865.6 K	Ψ	550
R_l	0.0824	B_φ	1.5
R_g	0.745	Q_c	10^{28} kJ/kg
γ_φ	0.01 kg m/s^2	μ_f	0.0004 kg/m · s

Table 2 Parameters for unsteady calculation of melt-layer-front growth and propagation

Parameter	Value	Parameter	Value
ρ_1	1800 kg/m^3	Q_m	−300 kJ/kg
u_1	0 m/s	Q_v	−1800 kJ/kg
T_1	865 K	c_v	1 kJ/kg · K
φ_1	10^{-14}	κ	0.4 W/m · K
p_1	0.417 MPa	Ψ	550
T_m	580.1 K	B_φ	1.5
T_v	865.6 K	Q_c	3×10^{15} kJ/kg
R_l	0.0824	R_g	0.745

$Q_c\beta_c$, as used in the two-step chemical kinetics, is illustrated in [3], and further details can be found in [17].

The resulting system of ordinary differential equations is integrated using a fourth-order-explicit Runge–Kutta solver across the uniform end states of the melt-layer front ($-\infty < \xi < +\infty$).

D. Unsteady Calculation of Melt-Layer-Front Initiation, Growth, and Propagation

The full conservation equations of mass, momentum, energy, and the phase evolution in Eqs. (3–6) are solved. The unsteady motion of a melt-layer front is divided into three steps: initiation, growth, and propagation. The melt-layer initiation occurs upon ignition of the solid-state propellant. Across the melt-layer front, density experiences a sharp gradient, going from the condensed to the gaseous side. Following the initiation, the thickness of the hot melt-layer front grows until reaching a uniform thickness. Because the melt-layer thickness depends on pressure, the thickness during the growth step is much thicker than that observed during the propagation step. As the surface regression progresses, the pressure also rises as the flame

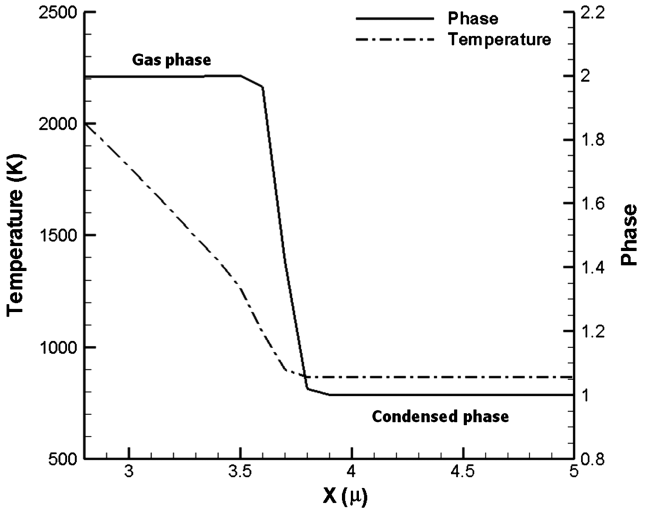

Fig. 8 Temperature profile shown during propagation step of melt-layer front.

Table 3 Computed and experimental burning rates at 100 bar

Parameter	Value
77.5% AP, calculated [4]	3.0 cm/s
80% AP, experiment [15]	4.5 cm/s
88% AP, calculated [in this work]	6.4 cm/s

temperature increases. When the ambient pressure is high, the melt-layer thickness is thin; when the ambient pressure is low, the melt-layer thickness is thick. The melt layer maintains uniform thickness as it propagates after the initiation and growth steps.

The discretized system of partial differential equations is solved in simultaneous steps of space and time integration. The spatial fluxes are first treated with the fourth-order convex essentially non-oscillatory scheme, and the resulting temporal ordinary differential system is solved by a third-order Runge–Kutta method. The details of numerical methodology are discussed in [18].

III. Results

The thickness of the melt layer (a whole layer of liquid state) is a fraction of 1 μ at 1 bar and 0.1 μ at a typical rocket chamber pressure of 100 bar. The present estimation gives the thickness on the order of 10^{-2} μ, as shown in Fig. 4, because it is the melt-layer front and not the whole layer thickness that is calculated. There are sharp gradients in phase field and density in the steady-state analysis. The two equilibrium end states of the steady-state phase analysis are 1) the liquid phase ($\varphi = 1$) on the left side and 2) the gas phase ($\varphi = 2$) on the right side, for the present layer front analysis. The literature values of the density of AP propellant are 1957 kg/m^3 at solid state, 1756 kg/m^3 at liquid state, and 8 kg/m^3 at gas state [8], while the present calculation provides an estimated condensed-phase density of ~1800 kg/m^3, as shown in Fig. 4.

Figures 5–7 show numerical solutions of the unsteady melt-layer-front propagation of AP propellant. During the burning of propellant, the liquid phase ($\varphi = 1$) is heated until a flame is sustained, and the melt layer is formed, as shown in Fig. 5. The left side is a gas phase, and the right side is a liquid phase, as the melt front propagates from left to right. Shown in the figure is a kink in the phase profile near $\varphi = 1.5$. Because the phase potential function constitutes three possible roots at $\varphi = 1$, 1.57, and 2, and $\varphi = 1.57$ is an unstable root denoting a quasi-stable state of the phase transition. As the propellant temperature rises during the progress of burning, the surface state shifts from condensed to gas phase, and the resulting melt front becomes the interface between condensed and gas, as illustrated in Figs. 6 and 7. The melt-layer front propagates at a uniform velocity upon completion of the growth step. The melt front of the AP propellant is thinner during the propagation step than the initiation step. During combustion, flame temperature rises and effectively elevates the chamber pressure, thus affecting the melt-front thickness. So the melt-layer thickness is thin when pressure is high and becomes thicker when pressure is low. The model parameters of melt-layer growth and propagation are summarized in Tables 1 and 2.

The propagation velocity is dependent on the surface temperature T_s according to [3,4], and it is given by

$$r = A \exp(-E_a/RT_s) \tag{12}$$

The surface temperature of 1150 K from Fig. 8, the activation energy E_a of 22 kcal/mol, and the preexponential factor A of 9.82×10^4 cm/s give the propagation velocity of 6.4 cm/s, which is a reasonable estimation, since 3 cm/s at 77.5% AP and 4.5 cm/s at 80% AP are reported by [4,15]. Table 3 summarizes computed and experimental velocities of AP propellant at 100 bar.

IV. Conclusions

Unlike most other works on propellant combustion simulation that targeted a single-phase propellant, be it the gas phase or condensed phase, our model directly solved the phase change by conservation

equations and a phase-field evolution equation that captured the initiation, growth, and propagation of the melt-layer front of the AP propellant. Even though there is no measured melt-layer-front thickness of AP-based propellant, we can provide thickness estimation through the available melt-layer information provided by [8]. Also, the calculated burning rate is in agreement with the experimentally measured velocity.

Although the present analysis considered the two-step phase-change mechanism from condensed to gas phase for evaluation of the melt layer, a full combustion mechanism may be coupled to the full governing equations to better represent the realistic surface burn process. However, the present approach is useful in evaluating the melt-layer-front thickness during AP propellant combustion. Furthermore, the present findings will help understand the complex burning characteristics of propellants. In particular, an accurate description of the layer's structure and its thickness would offset inaccuracies associated with the sonic measurement of the burn rate and consequently provide a more reliable measurement of the regression of AP/HTPB propellant.

Appendix

List of φ-dependent functions for $1 \le \varphi \le 2$:

$$F(\varphi) = [(\varphi - 1)(\varphi - 2)]^2 \tag{A1}$$

$$F'(\varphi) = 2(\varphi - 1)(\varphi - 2)(2\varphi - 3) \tag{A2}$$

$$\beta'_v(\varphi) = \begin{cases} 6(\varphi - 1)(2 - \varphi) & \text{for } 1 \le \varphi \le 2 \\ 0 & \text{otherwise} \end{cases} \tag{A3}$$

$$R(\varphi) = 2(R_{\text{liquid}} - R_{\text{gas}})(\varphi - 1)^3 - 3(R_{\text{liquid}} - R_{\text{gas}})(\varphi - 1)^2 + R_{\text{liquid}} \tag{A4}$$

$$R_{\text{liquid}}(\varphi) = 2R_l(\varphi - 1)^3 - 3R_l(\varphi - 1)^2 + R_l \tag{A5}$$

$$R_{\text{gas}}(\varphi) = -2R_g(\varphi - 1)^3 + 3R_g(\varphi - 1)^2 \tag{A6}$$

$$\beta_c(\varphi) = (5 - 2\varphi)(\varphi - 1)^2 \tag{A7}$$

Acknowledgments

This research was supported by the Agency for Defense Development (ADD) Basic Research (08-08-01) and ADD grants (042-20080050) through the Institute of Advanced Aerospace Technology and the Engineering Research Institute at Seoul National University. Useful discussions with J. C. Yoo, C. K. Kim, and Y. D. Doh of the Core Technology Group at ADD are warmly acknowledged.

References

[1] Hermance, C. E., "A Model of Composite Propellant Combustion Including Surface Heterogeneity and Heat Generation," *AIAA Journal*, Vol. 4, No. 9, 1966, pp. 1629–1637. doi:10.2514/3.55284

[2] Beckstead, M., Derr, R., and Price, C., "A Model of Composite Solid-Propellant Combustion Based on Multiple Flames," *AIAA Journal*, Vol. 8, No. 12, 1970, pp. 2200–2207. doi:10.2514/3.6087

[3] Hegab, A., Jackson, T. L., Buckmaster, J., and Stewart, D. S., "Nonsteady Burning of Periodic Sandwich Propellants with Complete Coupling between the Solid and Gas Phases," *Combustion and Flame*, Vol. 125, Nos. 1–2, 2001, pp. 1055–1070. doi:10.1016/S0010-2180(01)00226-7

[4] Massa, L., Jackson, T. L., and Buckmaster, J., "New Kinetics for a Model of Heterogeneous Propellant Combustion," *Journal of Propulsion and Power*, Vol. 21, No. 5, 2005, pp. 914–924. doi:10.2514/1.2433

[5] Cai, W., Thakre, P., and Yang, V., "A Model of AP/HTPB Composite Propellant Combustion in Rocket-Motor Environments," *Combustion Science and Technology*, Vol. 180, No. 12, 2008, pp. 2143–2169. doi:10.1080/00102200802414915

[6] Jacobs, P. W. M., and Whitehead, H. M., "Decomposition and Combustion of Ammonium Perchlorate," *Chemical Reviews (Washington, DC)*, Vol. 69, No. 4, 1969, pp. 551–590. doi:10.1021/cr60260a005

[7] Jacobs, P. W. M., and Pearson, G. S., "Mechanism of the Decomposition of Ammonium Perchlorate," *Combustion and Flame*, Vol. 13, No. 4, 1969, pp. 419–430. doi:10.1016/0010-2180(69)90112-6

[8] Tanaka, M., and Beckstead, M., "A Three-Phase Combustion Model of Ammonium Perchlorate," AIAA Paper 1996-2888, 1996.

[9] Gurtin, M. E., "Generalized Ginzburg–Laudau and Cahn–Hilliard Equations Based on a Microforce Balance," *Physica. D: Nonlinear Phenomena*, Vol. 92, Nos. 3–4, 1996, pp. 178–192. doi:10.1016/0167-2789(95)00173-5

[10] Summerfield, M., Sutherland, G. S., Webb, M. J., Taback, H. J., and Hall, K. P., *Solid Propellant Rocket Research*, Academic Press, New York, 1960, pp. 141–182.

[11] Washburn, E., and Beckstead, M., "Modeling Multiphase Effects in the Combustion of HMX and RDX," *Journal of Propulsion and Power*, Vol. 22, No. 5, 2006, pp. 938–946. doi:10.2514/1.12689

[12] Liau, Y., and Yang, V., "Analysis of RDX Monopropellant Combustion with Two-Phase Subsurface Reactions," *Journal of Propulsion and Power*, Vol. 11, No. 4, 1995, pp. 729–739. doi:10.2514/3.23898

[13] Yoh, J. J., "Analysis of Phase Front Structures of Energetic Materials," *Journal of Physics: Condensed Matter*, Vol. 18, No. 35, 2006, pp. 8179–8193. doi:10.1088/0953-8984/18/35/006

[14] Beckstead, M. W., and Hightower, J. D., "Surface Temperature of Deflagrating Ammonium Perchlorate Crystals," *AIAA Journal*, Vol. 5, No. 10, 1967, pp. 1785–1790. doi:10.2514/3.4305

[15] Jeppson, M. B., Beckstead, M. W., and Jing, Q., "A Kinetic Model for the Premixed Combustion of a Fine AP/HTPB Composite Propellant," *AIAA Proceedings of the 35th Jannaf Combustion Meeting*, Vol. 33, 1998, pp. 639–653.

[16] Ruderman, G. A., Stewart, D. S., and Yoh, J. J., "A Thermomechanical Model for Energetic Materials with Phase Transformations," *SIAM Journal on Applied Mathematics*, Vol. 63, No. 2, 2002, pp. 510–537. doi:10.1137/S0036139901390258

[17] Gwak, M. C., Jung, T. Y., and Yoh, J. J., "Friction-Induced Ignition Modeling of Energetic Materials," *Journal of Mechanical Science and Technology*, Vol. 23, No. 7, 2009, pp. 1779–1787. doi:10.1007/s12206-009-0603-1

[18] Kim, K. H., and Yoh, J. J., "Shock Compression of Condensed Matter Using Multimaterial Reactive Ghost Fluid Method," *Journal of Mathematical Physics*, Vol. 49, No. 4, 2008, Paper 043511. doi:10.1063/1.2905152

S. Son
Associate Editor